Available online at www.sciencedirect.com

SciVerse ScienceDirect

journal homepage: www.elsevier.com/locate/he

Production of ultrapure hydrogen in a Pd–Ag membrane reactor using noble metals supported on La–Si oxides. Heterogeneous modeling for the water gas shift reaction

Carolina A. Cornaglia [a], María E. Adrover [b], John F. Múnera [a], Marisa N. Pedernera [b], Daniel O. Borio [b], Eduardo A. Lombardo [a,*]

[a] Instituto de Investigaciones en Catálisis y Petroquímica – INCAPE (FIQ, UNL-CONICET), Santiago del Estero 2829, 3000 Santa Fe, Argentina

[b] PLAPIQUI – UNS/CONICET, Camino La Carrindanga km 7, 8000 Bahía Blanca (BA), Argentina

ARTICLE INFO

Article history:
Received 20 February 2013
Received in revised form
26 April 2013
Accepted 6 May 2013
Available online 24 June 2013

Keywords:
H_2 production
H_2 purification
Pt catalysts
Mass transfer limitations

ABSTRACT

Two different catalysts, Rh(0.6% wt/wt)/La_2O_3(27% wt/wt)·SiO_2 and Pt(0.6% wt/wt)/La_2O_3(27%)·SiO_2, were tested in the WGS reaction. Their performances were first studied in a conventional fixed-bed reactor. Their activities were similar and they were both very stable. However, as Pt(0.6)/La_2O_3(27)·SiO_2 showed a much higher selectivity to the desired reaction, the performance of a membrane reactor employing this catalyst was studied. The effects of the H_2O/CO ratio, space velocity, sweep gas flow rate and size of the catalyst particle on CO conversion and H_2 recovery were studied at laboratory scale under isothermal conditions. A 1-D heterogeneous model was developed in order to properly reproduce the experimental results obtaining good agreement between the simulation results and laboratory data. The experimental and theoretical results confirm the existence of significant external mass-transfer limitations in the fluid-particle interface for these very active formulations.

1. Introduction

Hydrogen production has been extensively studied in the last two decades as a key element of the energy matrix. Hydrogen is industrially obtained from the steam reforming of natural gas or heavier hydrocarbons. In the case of fuel cell applications, this hydrogen stream needs to be purified by means of the water gas shift reaction (WGSR) usually conducted in one or two steps, and CO Preferential Oxidation (CO-PrOx) to avoid poisoning of the PEM fuel-cell anode catalyst. Since the WGS reaction rate is slower than the other reactions involved in the steam reforming process, and is limited at high temperatures by the thermodynamic equilibrium, the WGS reactor is the largest and heaviest process component [1]. A similar situation occurs in the case of fuel processors used to produce pure H_2 in situ to feed a PEM fuel cell [2]. An attractive alternative is to conduct the WGSR in a membrane reactor (MR), using only one vessel to

* Corresponding author. Tel./fax: +54 342 4536861.
E-mail address: nfisico@fiq.unl.edu.ar (E.A. Lombardo).

0360-3199/$ – see front matter
http://dx.doi.org/10.1016/j.ijhydene.2013.05.043

obtain ultrapure hydrogen. In this work, a commercial dense Pd membrane is used to obtain pure H_2 (<10 ppm CO) reaching conversion values above equilibrium. In order to increase the permeation through the membrane, a sweep gas (SG) stream (i.e. Argon) is employed. In a practical application, the sweep gas should be overheated steam to facilitate separation.

Ma and Lund [3] suggested that the reaction rate is the rate-limiting step in a membrane reactor operating adiabatically where the WGS reaction is carried out at high temperatures using catalysts based on Fe/Cr. For this reason, in recent years numerous papers have been published concerning the development of more active catalysts. A key factor is the stability of the well-performing supported noble metal formulations shown in the current literature. Several studies have been published concerning the use of Pt catalysts in the WGSR but only a few of them include stability data [4]. Panagiotopolou and Kondarides have reported that Pt/TiO_2, Pt/CeO_2 and Pt/CeO_2–TiO_2 catalysts display a strong metal support interaction, showing the best performance. As a matter of fact, few papers provide data about deactivation of WGS catalysts. Concerning this point, a recent review [5] highlights the need to report relevant deactivation data of promising catalysts to evaluate their practical use. Bi et al. [6] performed the WGS reaction catalyzed by $Pt/Ce_{0.6}Zr_{0.4}O_2$ in a membrane reactor employing a supported palladium membrane with a thickness of 1.4 μm. The authors emphasized the development of catalysts with faster kinetics than the commercial formulations. Although their catalyst complied with this condition at temperatures above 623 K, no data were provided about its stability-deactivation behavior. Note that the minimum temperatures at which the Pd membrane can efficiently operate are 623–673 K. At lower temperatures, the strongly adsorbed CO reduces the H_2 flow through the membrane, while higher temperatures affect its durability.

Most theoretical studies focused on membrane reactors for the WGS have proposed isothermal mathematical models [7–9]. However, when higher reactor scales are under consideration, the thermal effects should be taken into account [10–12]. All these isothermal and non-isothermal models assume negligible mass-transfer resistances on the gas–solid interface. Certainly, the use of pseudohomogeneous mathematical models is appropriate to reproduce experimental results when the controlling step is the catalytic reaction. However, for other operating conditions (e.g., in the presence of high catalyst activities and/or for the typical low process flow rates used at laboratory scale) the influence of the mass transfer limitations should be taken into account by means of heterogeneous models.

The aim of the present study was to develop a heterogeneous approach to model the behavior of a lab membrane reactor using a very active noble metal supported formulation. Newly developed Rh [13] and Pt catalysts – active, selective, stable and non-carbon forming – were used in the membrane reactor. The influence of the main operating and design variables (space velocity, sweep gas flow rate, catalyst particle diameter) on the CO conversion and H_2 recovery in the membrane reactor was analyzed.

2. Experimental

2.1. Catalyst preparation

The $La_2O_3{\cdot}SiO_2$ support was prepared by incipient wetness impregnation of SiO_2 with lanthanum nitrate (Anedra). The SiO_2 (Aerosil 300) employed in the solid preparation was previously calcined at 1173 K. The solids were calcined at 873 K. After calcination the load of lanthanum given as La_2O_3 was 27 wt%. The Pt and Rh supported catalysts were prepared by incipient wetness impregnation using $Pt(NH_3)_4{\cdot}Cl_2{\cdot}H_2O$ (Strem Chemicals, Inc., 99.95%-Pt) and $RhCl_3{\cdot}6H_2O$ (Alfa Aesar, 99.99%) as precursors. The samples were kept at room temperature for 4 h and then dried at 343 K overnight. The apparent densities of both catalysts were the same: 0.5 g/cm^3.

Prior to use, both catalysts were ground to a particle size lower than 20 μm (verified by SEM). In the Pt containing formulation, in order to obtain larger catalyst particles (230 μm), the solid was pressed and sieved to the required size.

2.2. Catalyst characterization

The fresh-reduced and used (after exposure to WGSR conditions) catalysts were analyzed by X-Ray Diffraction (XRD) using an XD-D1 Shimadzu instrument and Cu Kα radiation at 30 kV and 40 mA. The scanning rate was 1.0°/min for values between $2\theta = 10°$ and 60°. BET surface areas (S_g) were measured by N_2 physisorption at its boiling point in a Micromeritics Accusorb 2100 E sorptometer.

The Raman spectra of fresh and used solids were recorded using a LabRam spectrometer (Horiba-Jobin-Yvon) coupled to an Olympus confocal microscope (a 100× objective lens was used for simultaneous illumination and collection), equipped with a CCD detector cooled to about 200 K using the Peltier effect. The excitation wavelength was in all cases 532 nm (Spectra Physics diode pump solid state laser). The laser power was set at 30 mW.

2.3. Catalytic measurements

2.3.1. Conventional fixed-bed reactor

Catalytic measurements were conducted in a conventional flow system isothermally operated at atmospheric pressure. The tubular quartz reactor had an inner diameter of 9.5 mm, the same as the membrane reactor. The feed stream gas mixture was made up of CO (Linde, 2.3), H_2O (distilled) and Ar (Indura S.A., 5.0). CO and Ar were controlled using MKS mass flow controllers, while the steam was generated in a preheater fed with water from a syringe pump (Apema S.R.L.) at the desired flow rate. The reaction temperature was controlled through a thermocouple placed inside the catalyst bed. The catalysts were heated in Ar at 673 K at a rate of 1.5 K min^{-1}, afterward they were reduced in flowing H_2 (Indura S.A., 5.0) at the same temperature for 2 h. The reaction was carried out at 673 K and the feed stream gas mixture was made up of CO and H_2O ($H_2O/CO = 2–3$). The reactor was operated in both differential and integral modes. The gases leaving the reactor flowed through an ice-cooled trap and a tube packed with silica gel to remove water before the gas chromatographic

analysis. The feed and product streams were analyzed with a Shimadzu 9A thermal conductivity detector (TCD) gas chromatograph equipped with a Hayezep D column for the complete separation of the gaseous components.

2.3.2. *Membrane reactor*

The reaction was carried out using a double tubular membrane reactor isothermally operated at 673 K and atmospheric pressure (Fig. 1).

The membrane reactor was built using a commercial dense Pd–Ag alloy (inner tube, 50 μm thick) provided by REB Research and Consulting, with one end closed and an inner tube to feed sweep gas, i.e. Ar. The outer tube was made of commercial non-porous quartz. The catalyst was packed in the annular region. The design parameters are shown in Table 1. The membrane was 100% selective, so only hydrogen was detected on the permeate side, even after several hundred hours on stream under reaction conditions.

Table 1 – Design parameters and operating conditions of the membrane reactor.

Design parameters				Operating conditions	
L	73 mm	W_{cat}	150 mg	H_2O/CO	2–3
L_m	70 mm	W_{inert}	5000 mg	F_{SG}	0–200 N ml min^{-1}
d_{te}	3.2 mm	d_p	20 or 230 μm	Pressure	1 atm
d_s	9.5 mm	Membrane area	7.0 cm^2	Temperature	673 K

3. Mathematical model

A heterogeneous 1-D model was selected to represent the steady state operation of the laboratory membrane reactor. Under these conditions, the modeling of MRs presents interesting challenges because of the coupling of H_2 selective diffusion through the membrane with chemical reaction and mass transfer in the gas–solid interface.

The following assumptions were made: isobaric and isothermal conditions; axial dispersion phenomena are neglected; temperature and composition gradients in the radial coordinate are also neglected. Unlike all previous modeling studies about WGSR in membrane reactors [5], the gas–solid mass transfer resistances were taken into account. Due to the non-porous nature of the catalyst support, the internal mass transfer resistances were neglected. Only H_2 permeated (100% selectivity).

Consistent with these assumptions, the governing equations for the retentate and permeate sides are given below:

Retentate side (shell side):

Mass Balances

Gas phase:

$$\frac{dX_{CO}}{dz} = \frac{A_T}{F_{CO,o}} k_{g,CO} a_v \left(p_{CO} - p_{CO}^S\right) \quad (1)$$

$$\text{where} \quad A_T = \frac{\pi}{4}\left(d_s^2 - d_{te}^2\right) \quad (2)$$

Solid phase:

$$\rho_b \, r_{CO}\left(p_i^S\right) = k_{g,CO} a_v \left(p_{CO} - p_{CO}^S\right) \quad (3)$$

$$\text{where :} \quad a_v = \frac{S_g W}{V_r} \quad (4)$$

The reaction rate in Eq. (3) is evaluated at the partial pressures corresponding to the catalyst surface. Considering the reaction stoichiometry and the permeated hydrogen flow rate, the fluid-phase compositions of all components involved in the reaction are,

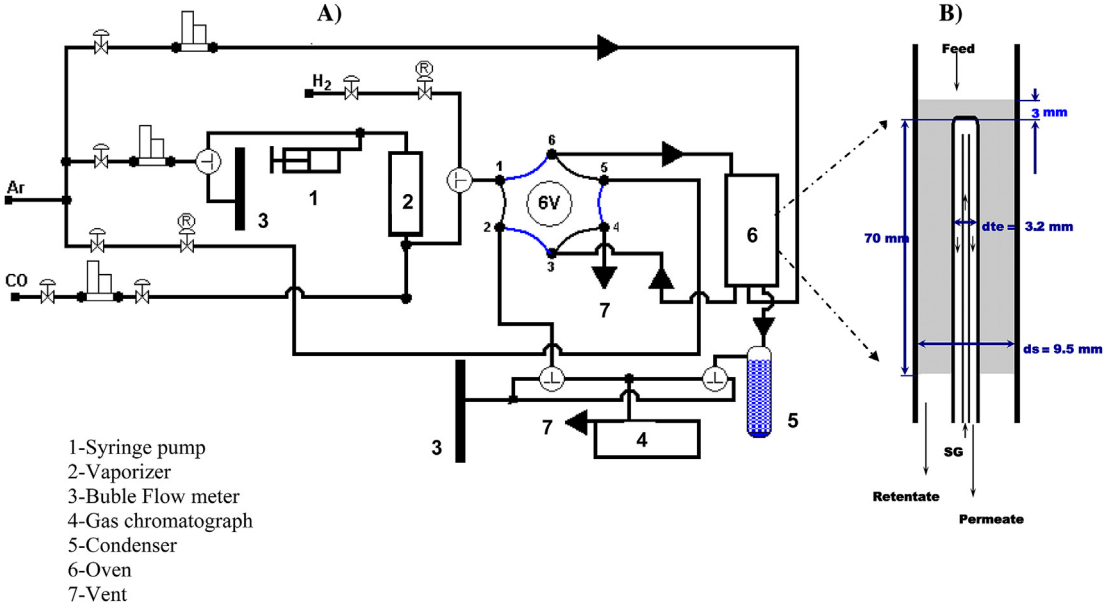

Fig. 1 – A) Flow sheet of the reaction system. B) Membrane reactor SG (sweep gas).

$$y_{H_2} = \frac{F_{H_2,o} + F_{CO,o}X_{CO} - F_{H_2,P}}{F_{To} - F_{H_2,P}} \quad (5)$$

$$y_{H_2O} = \frac{F_{H_2O,o} - F_{CO,o}X_{CO}}{F_{To} - F_{H_2,P}} \quad (6)$$

$$y_{CO_2} = \frac{F_{CO_2,o} + F_{CO,o}X_{CO}}{F_{To} - F_{H_2,P}} \quad (7)$$

$$y_{CO} = \frac{F_{CO,o}(1 - X_{CO})}{F_{To} - F_{H_2,P}} \quad (8)$$

Once the molar fractions are estimated for the fluid phase, the surface partial pressures of all components are:

$$p^S_{H_2O} = p_{H_2O} - \frac{k_{g,CO}}{k_{g,H_2O}}(p_{CO} - p^S_{CO}) \quad (9)$$

$$p^S_{CO_2} = p_{CO_2} + \frac{k_{g,CO}}{k_{g,CO_2}}(p_{CO} - p^S_{CO}) \quad (10)$$

$$p^S_{H_2} = p_{H_2} + \frac{k_{g,CO}}{k_{g,H_2}}(p_{CO} - p^S_{CO}) \quad (11)$$

The mass transfer coefficients are calculated employing correlations obtained from the literature [14]:

$$k_{g,i} = \frac{0.357 Re_p^{-0.359} G}{\varepsilon P M S c_i^{2/3} P} \quad 3 < Re_p < 2000 \quad (12)$$

Permeate side (tube side):

Mass Balances

$$\frac{dF_{H_2,P}}{dz} = \pi d_{te} J_{H_2} \quad (13)$$

Boundary conditions:

$$\text{At } z = 0 \begin{cases} F_i = F_{io} \quad \text{for } i = 1, 2\ldots, N \\ T = T_o = T_P \\ F_{H_2,P} = 0;\ F_{SG} \neq 0 \end{cases} \quad (14)$$

Surface partial pressures are obtained by iteratively solving the set of algebraic equations using the Broyden method [15]. At the same time, both the CO conversion and the permeated hydrogen flow rate were obtained integrating the differential Eqs. (1 and 13) by means of the Gear algorithm [16].

The design parameters and the operating conditions used in the simulations are shown in Table 1.

4. Results and discussion

4.1. Stability tests

The stability tests for the Pt(0.6)/La_2O_3(27)·SiO_2 catalyst were performed in the conventional fixed bed reactor at 673 K, 1 atm, H_2O/CO = 2–3, d_p = 20 μm and GHSV = $F_{To}/W = 6.7 \times 10^6$ ml g^{-1} h^{-1}. This high space velocity was required to eliminate external mass transport limitations [13]. As shown in Fig. 2, Pt(0.6)/La_2O_3(27)·SiO_2 was stable for at least 50 h on stream. The reaction rate values were 0.028 mol g^{-1} min^{-1} (H_2O/CO = 3) and 0.018 mol g^{-1} min^{-1} (H_2O/CO = 2).

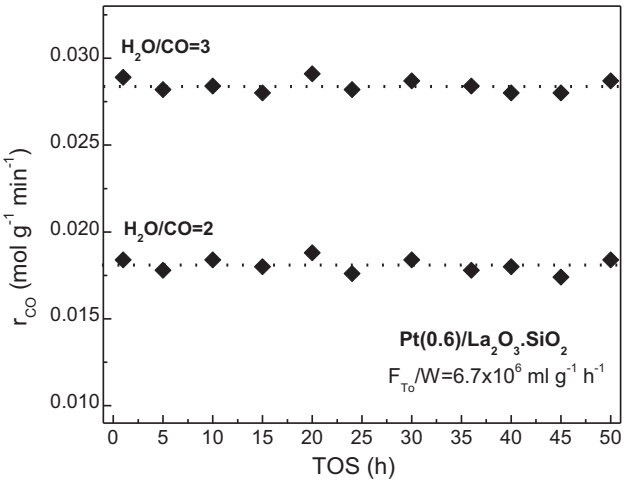

Fig. 2 – Stability test for the Pt(0.6)/La_2O_3(27)·SiO_2 solid (d_p = 20 μm) at 673 K at different H_2O/CO ratios, $F_{To}/W = 6.7 \cdot 10^6$ ml g^{-1} h^{-1}, P = 1 atm.

The stability of the Rh(0.6)/La_2O_3(27)·SiO_2 catalyst was reported in a previous work [13]. This solid showed a constant reaction rate of 0.0165 mol g^{-1} min^{-1} with H_2O/CO = 3 for the same period on stream, under similar reaction conditions.

4.2. Catalyst characterization

The XRD pattern of fresh Pt(0.6)/La_2O_3(27)·SiO_2 (Fig. 3) shows broad peaks centered around 2θ = 28° and 45° (extremely weak) which correspond to the lanthanum disilicate phase

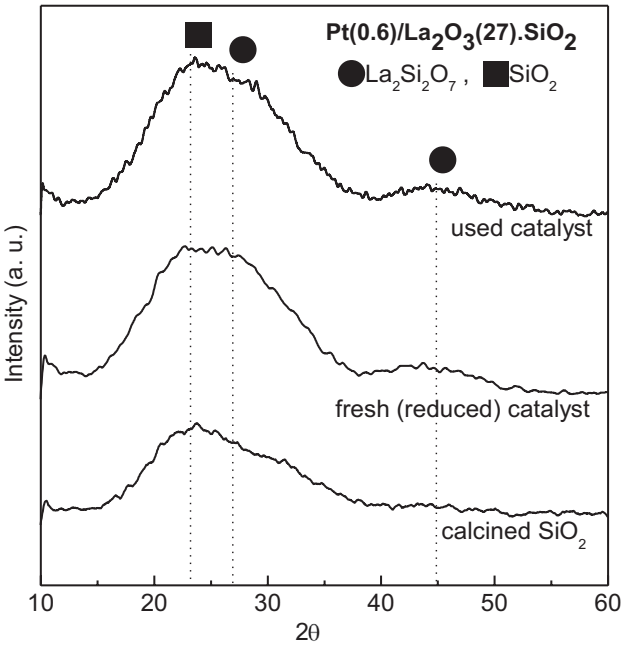

Fig. 3 – XRD patterns for the fresh and used Pt(0.6)/La_2O_3(27)·SiO_2 catalysts (after being on stream at T = 673 K, P = 1 atm and H_2O/CO = 3).

$La_2Si_2O_7$, as previously reported by Vidal et al. [17]. Note that the diffractograms of the freshly prepared catalysts and after use in WGSR are very similar; however, slightly different intensities of the peaks are displayed.

The pattern of the calcined SiO_2 shows a broad peak approximately at $2\theta = 23°$. This peak can be observed in the XRD pattern of the fresh and used catalysts. Therefore, both the $La_2Si_2O_7$ and SiO_2 phases are observed in the Pt(0.6)/La_2O_3(27)·SiO_2 catalyst. In a previous work [13], the Rh(0.6)/La_2O_3(27)·SiO_2 solid contained the same $La_2Si_2O_7$·SiO_2 phase which remained unchanged after the WGS reaction.

The Raman spectrum of the used Pt(0.6)/La_2O_3(27)·SiO_2 catalyst (not shown) does not show any bands corresponding to the presence of either graphitic residues, carbonates or formates. Since the $La_2Si_2O_7$ phase shows very low cristallinity (Fig. 3), it does not have Raman active bands.

The Raman spectrum of the used Rh(0.6)/La_2O_3(27)·SiO_2 catalyst reported the presence of small amounts of graphitic carbon [13]. Note that these tiny amounts of carbon, undetected by TGA, do not affect the high stability of this formulation.

4.3. Conventional fixed-bed reactor

Both the Rh(0.6)/La_2O_3(27)·SiO_2 and the Pt(0.6)/La_2O_3(27)·SiO_2 solids were evaluated in a conventional fixed-bed reactor under space velocities similar to those used in the membrane reactor (GHSV = 6–24·10^3 ml g^{-1} h^{-1}). The reaction was carried out at 673 K and the feed stream gas mixture was made up of CO and H_2O (H_2O/CO = 3).

Fig. 4 shows that the Pt(0.6)/La_2O_3(27)·SiO_2 catalyst is highly selective to the WGS reaction, while the Rh(0.6)/La_2O_3(27)·SiO_2 solid presents a significant selectivity to methane. Note that the selectivity to methane of the platinum catalyst is negligible. Particularly, at the lowest space velocity, the Pt(0.6)/La_2O_3(27)·SiO_2 catalyst shows a high selectivity to the WGSR (S_{WGS} = 99.8%) while the Rh(0.6)/La_2O_3(27)·SiO_2 solid does not (S_{WGS} = 82.1%). Due to the high activity of the Pt catalyst, the CO conversion is close to the equilibrium value for the whole range of space velocities, which is in agreement with the results reported by Bi et al. [6]. Also note that when the Rh formulation is used, the measured CO conversion is above the calculated equilibrium value for the single WGSR because of the simultaneous occurrence of the irreversible and undesirable methanation reaction.

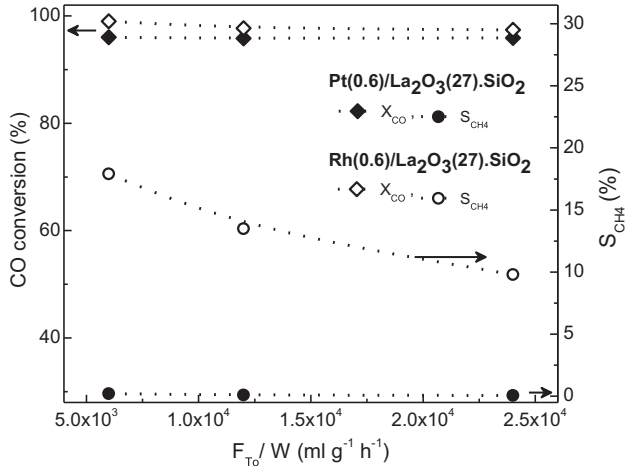

Fig. 4 – Effect of space velocity upon the CO conversion and CH_4 selectivity (S_{CH_4}) in the conventional reactor. T = 673 K, P = 1 atm and H_2O/CO = 3 (Equilibrium CO conversion = 96.2%).

4.4. Membrane reactor

Since Pt(0.6)/La_2O_3(27)·SiO_2 is a very active, stable, selective and non-carbon forming catalyst, it was selected for use in the membrane reactor. The catalyst stability was again checked in the membrane reactor because, under these conditions, the solid is operating at lower hydrogen partial pressure than in the conventional reactor under integral regime. The test was performed during 100 h and no variation in catalyst activity was observed. The WGS selectivity remained constant at almost 100%.

The effects of the H_2O/CO ratio and sweep-gas flow rate (F_{SG}) upon the reactor performance were studied.

4.4.1. Effect of the H_2O/CO ratio

The effect of the H_2O/CO ratio was studied at 673 K employing a sweep gas flow rate of 100 N ml min^{-1} and a space velocity of 6.0 × 10^3 ml g^{-1} h^{-1}. In Fig. 5, the hydrogen recovery shows a relative increase of 11.2% when the H_2O/CO ratio decreases from 3 to 2. This is due to an increase of the H_2 partial pressure gradient (approximately 9%, calculated as an average of the H_2 partial pressure gradient between the beginning and end of the membrane). Nevertheless, the CO conversion shows a slight drop when the excess of water decreases because the chemical equilibrium is shifted to the left.

4.4.2. Effect of the sweep gas flow rate

Fig. 6 confirms that both the CO conversion and the H_2 recovery reached a plateau value at F_{SG} near 150 N ml min^{-1}.

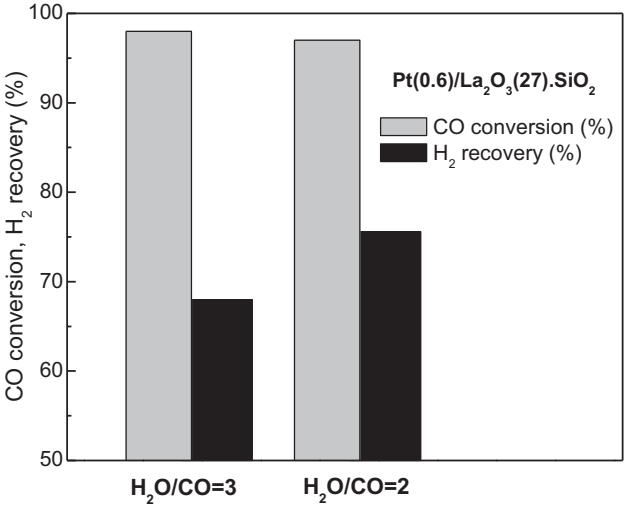

Fig. 5 – Membrane reactor: Effect of the H_2O/CO ratio over the CO conversion and the hydrogen recovery for the Pt(0.6)/La_2O_3(27)·SiO_2 (d_p = 20 μm), T = 673 K, P = 1 atm, F_{To}/W = 6.0 × 10^3 ml g^{-1} h^{-1}, F_{SG} = 100 N ml min^{-1}.

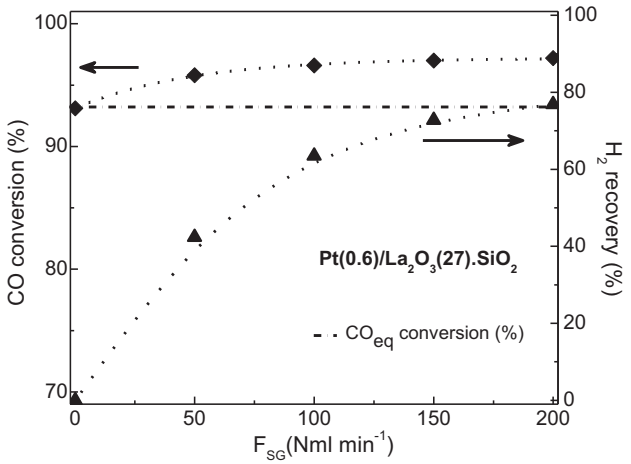

Fig. 6 – Effect of F_{SG} on the performance of the Pt(0.6)/La_2O_3(27)·SiO_2 solid. $T = 673$ K, $P = 1$ atm, $H_2O/CO = 2$ and ($F_{To}/W = 1.8 \times 10^4$ ml g^{-1} h^{-1}).

When $F_{SG} = 0$, the reaction reached the theoretical equilibrium conversion value (93.1%). Note that without sweep gas flow, the system operates as a conventional reactor. The increase of the Ar sweep gas flow reduces the hydrogen partial pressure on the permeate side leading to a higher H_2 flow rate through the membrane. Note that the CO conversion is just moderately improved by the sweep gas flow rate because the system is operating at high conversion levels. For other operating conditions, such as higher space velocities or feed streams rich in H_2 [18–21], the influence of the sweep gas flow rate on the conversion becomes more significant.

4.5. *Mathematical model applied to Pt(0.6)La_2O_3(27)·SiO_2*

4.5.1. *Reaction kinetics*

The Langmuir–Hinshelwood rate equation used to model the membrane reactor with the Pt(0.6)/La_2O_3(27)·SiO_2 formulation was adapted from that obtained for a Rh catalyst operating under the differential mode [13]:

$$-r_{CO} = \frac{kK_{CO}K_{H_2O}p^s_{CO}p^s_{H_2O}}{\left(1 + K_{CO}p^s_{CO} + K_{H_2O}p^s_{H_2O} + \sqrt{K_{H_2}p^s_{H_2}}\right)^2}\left(1 - \frac{p^s_{H_2}p^s_{CO_2}}{p^s_{H_2O}p^s_{CO}K}\right) \quad (15)$$

This approach could be justified because the Pt and Rh noble metals have a similar catalytic behavior. Also, both catalysts were prepared with the same support ($La_2Si_2O_7$·SiO_2) and employing the identical load of noble metal (0.6 wt%). A corrective term was included in the numerator of Eq. (15) to account for the effect of the reverse WGSR, a new term was also included in the denominator to consider the adsorption of H_2, which is not negligible under integral mode. The average activity of the Pt catalyst was adapted by means of a fitting procedure based on experimental data. The kinetic parameters used in the reactor model are reported in Table 2.

Table 2 – Kinetic parameters used in the reactor model.

k	$1.39 \cdot 10^{13} \cdot e^{(-18600/T)}$	mol_{CO} kg^{-1}_{cat} s^{-1}
K_{CO}	$6.85 \cdot 10^{-12} \cdot e^{(15540/T)}$	kPa^{-1}
K_{H_2O}	$1.83 \cdot 10^{-9} \cdot e^{(10850/T)}$	kPa^{-1}
K_{H_2}	$4.25 \cdot 10^{-7} \cdot e^{(9334/T)}$	kPa^{-1}
K [22]	$e^{[(4577.8/T)-4.33]}$	

4.5.2. *Hydrogen permeation rate*

The permeation flow rate through the membrane follows Sievert's Law. The 0.0675 value was fitted at 673 K by measuring the H_2 flow rates permeated at different values of the driving force,

$$J_{H_2} = 0.0675\left(\sqrt{p_{H_2}} - \sqrt{p_{H_2,P}}\right) \quad (16)$$

4.6. *Comparison between model and experimental data*

4.6.1. *Effect of the space velocity*

Fig. 7 shows the effect of the space velocity on the CO conversion and H_2 recovery. Experimental data are indicated by symbols and the model predictions, obtained by means of the heterogenous model (Section 3), are indicated by lines. As expected, the experimental H_2 recovery shows a significant decrease at increasing space velocity. This trend is in agreement with that reported by Bi et al. [6] for the WGSR conducted in a Pd membrane reactor. As the space velocity increases (i.e., higher F_{To} values), a decrease in the contact time between the process gas and the Pd membrane occurs. These lower contact times cause the H_2 recovery to drop from 77% to 31%, for a total increase in the gas flow rate close to 4 times. In line with the decrease of H_2 recovery, the CO conversion drops with the space time for two main reasons: the equilibrium shifting caused by the Pd membrane becomes less important (lower H_2 recoveries take place) and the reactants residence time decreases. However, due to the high activity of the Pt catalyst, the conversion drop is not as severe as that corresponding to the H_2 recovery. In Fig. 7, it can be observed that the model reproduces the experimental measurements satisfactorily.

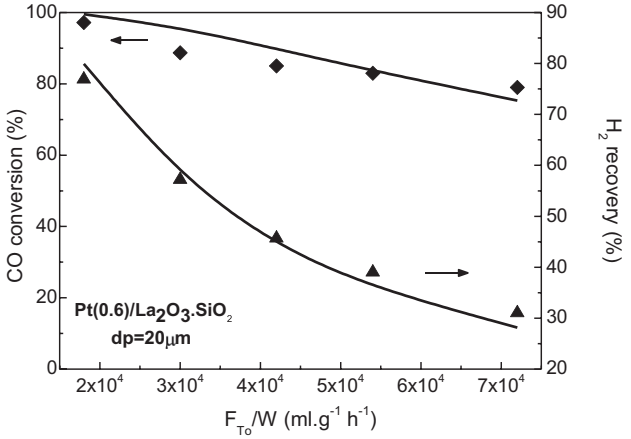

Fig. 7 – Effect of the space velocity (F_{To}/W) on the CO conversion and H_2 recovery using the Pt(0.6)/La_2O_3(27)·SiO_2 ($d_p = 20$ μm). $T = 673$ K, $P = 1$ atm, $H_2O/CO = 2$ and $F_{SG} = 200$ N ml min^{-1}. Points are experimental while curves are simulated.

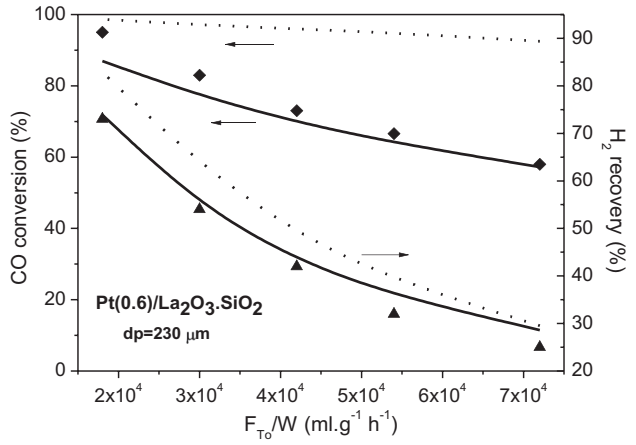

Fig. 8 – Effect of the space velocity (F_{To}/W) on the CO conversion and H_2 recovery using the $Pt(0.6)/La_2O_3(27)\cdot SiO_2$ (d_p = 230 μm). T = 673 K, P = 1 atm, H_2O/CO = 2 and F_{SG} = 200 N ml min^{-1}. Full lines: heterogeneous model, dotted line: pseudohomogeneous model.

4.6.2. *Analysis of the influence of particle diameter (d_p) on MR performance*

The influence of the particle diameter on the performance of the MR is analyzed in order to test the validity of the model. The design parameters and the experimental conditions remain the same as those already detailed in Table 1, except for d_p = 230 μm instead of 20 μm.

The effect of the space velocity on the CO conversion and H_2 recovery is shown in Fig. 8 for d_p = 230 μm. Experimental data are indicated by symbols and the heterogeneous model predictions by full lines. Note that the heterogeneous mathematical model satisfactorily reproduces the experimental tendencies. The comparison between Figs. 8 and 7 reflects that, as the d_p increases, the external particle surface area per unit reactor volume (a_v, Eq. (4)) decreases and the external mass transfer limitations become more important; consequently, the conversion levels significantly decrease. This fact confirms that the external mass transfer limitations in the membrane reactor cannot be neglected. Simulations by means of a pseudohomogeneous model were also performed, setting very high values of the mass transfer coefficients in the present model. In this case, the CO conversions (dottted lines in Fig. 8) and H_2 recoveries were overestimated and it was not possible to reproduce the effect of the particle size on the reactor performance experimentally observed.

Regarding the H_2 recovery, it also decreases with respect to that of smaller particles (compare Figs. 8 and 7). This phenomenon is associated with lower driving forces through the membrane for the case d_p = 230 μm, due to both the lower CO conversions (less H_2 is being generated) and the higher interfacial gradients, i.e., the bulk H_2 partial pressures (see Eq. (16)) become considerably lower than their values on the catalyst surface.

4.7. *Modeling of the partial pressure profiles inside the reactor*

Fig. 9 presents simulation results corresponding to axial profiles of the surface and bulk partial pressure for each

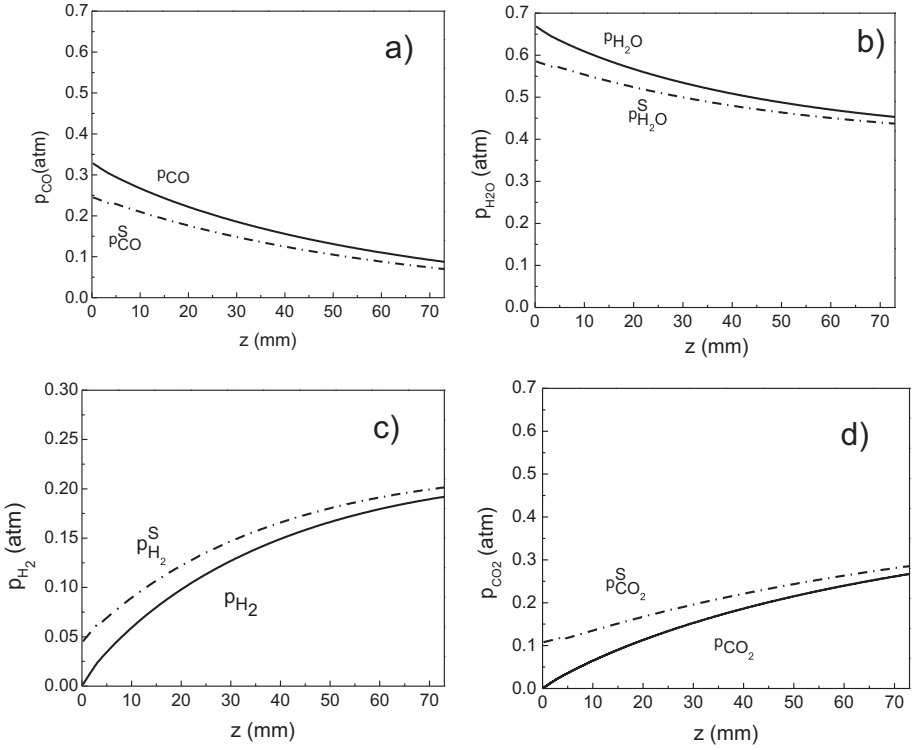

Fig. 9 – Simulated surface partial pressure axial profiles (dashed lines) and bulk partial pressure axial profiles (continuous lines) in the retentate corresponding to water (a), carbon monoxide (b), hydrogen (c) and carbon dioxide (d). These profiles correspond to $F_{To}/W = 7.2\cdot10^4$ ml g^{-1} h^{-1}.

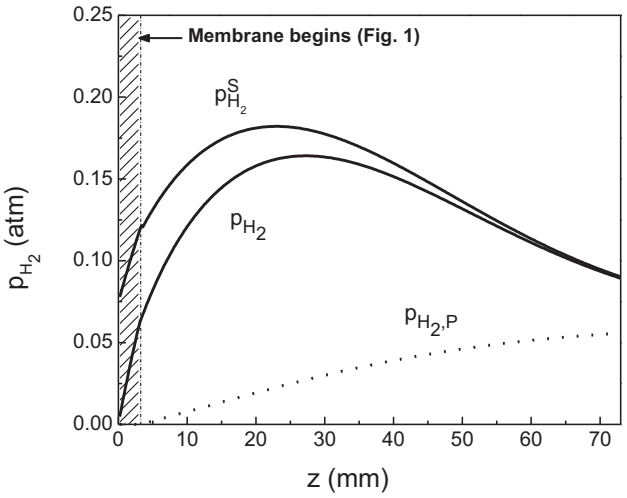

Fig. 10 – Simulated hydrogen bulk and surface partial pressure in the retentate side (continuous lines) and bulk partial pressure permeate side (dotted lines), $F_{To}/W = 1.8\cdot10^4$ ml g^{-1} h^{-1}.

component involved in the reaction. It can be observed that for the whole reactor length the surface partial pressures are higher than the bulk ones for reaction products. The reactants partial pressures profiles present the opposite behavior. These differences are accentuated near the reactor entrance due to higher reaction rates. Note as well that the modeling results included in Fig. 9 were obtained for the highest space velocity of those shown in Fig. 7, i.e., $F_{To}/W = 7.2\cdot10^4$ ml g^{-1} h^{-1}. For lower space velocities (e.g., lower values of the feed flow rate, F_{To}) the mass transfer coefficients (Eq. (12)) are smaller and the interfacial gradients become even more significant. This fact justifies the use of a heterogeneous model to simulate the range of operating conditions of the present study.

Fig. 10 shows hydrogen bulk partial pressure in the retentate (continuos lines) and permeate side (dotted lines) for a space velocity $F_{To}/W = 1.8\cdot10^4$ ml g^{-1} h^{-1}. Due to the low feed flow rate, a high H_2 recovery is reached (ca. 77%, see Fig. 7) and the partial pressure curves in the retentate side (bulk and surface) show a maximum. Downstream the maximum, the H_2 permeation rates through the membrane are higher than the H_2 generation rates by WGSR. In Fig. 9c, these maxima in the p_{H_2} and $p^s_{H_2}$ curves are not observed because the effect of the membrane on the reaction behavior is less significant (H_2 recovery of 30%). On the other side of the membrane, the resulting permeate stream is continuously enriched with hydrogen. For $z < 3$ mm, the hydrogen partial pressure in the permeate side ($p_{H_2,P}$) is zero because there is no membrane (See Fig. 1). If higher membrane areas were available, the values of p_{H_2} and $p_{H_2,P}$ would tend to coincide at the reactor outlet, the driving force in Eq. (16) would vanish and the H_2 recovery would converge to its maximum value for the chosen operating conditions.

5. Conclusions

The $Pt/La_2O_3{\cdot}SiO_2$ catalyst presented in this work is very active and selective for the WGSR and does not form carbonaceous residues. Not even traces of them were detectable by Laser Raman spectroscopy. Perhaps as a consequence of this absence of residues, the most remarkable feature of this catalyst is its stability for at least 100 h on stream.

The 1D heterogeneous model used in this work is shown to be required to simulate the performance of the membrane reactor used to produce 100% pure hydrogen varying the operating conditions. The model is able to predict the evolution of the CO conversion and hydrogen recovery with space velocity. It also correctly predicts the effect of catalyst particle size varying its average diameter between 20 and 230 μm. It was also shown that a 1D homogenous model is unable to reproduce the behavior of the membrane reactor when a very active catalyst is used. The proposed heterogeneous reactor model can be useful for a better understanding of the complex kinetic and transport phenomena involved in membrane reactors, with application to scale-up procedures and optimization studies.

Acknowledgments

The authors are grateful to Agencia Nacional de Promoción Científica y Tecnológica (ANPCyT), Consejo Nacional de Investigaciones Científicas y Técnicas (CONICET), Universidad Nacional del Litoral (UNL) and Universidad Nacional del Sur (UNS) for the financial support. Thanks are given to Elsa Grimaldi for the English language editing.

REFERENCES

[1] Francesconi JA, Mussati MC, Aguirre P. Analysis of design variables for water-gas-shift reactors by model-based optimization. J Power Sources 2007;173:467–77.
[2] Liu X, Ruettinger W, Xu X, Farrauto R. Deactivation of Pt/CeO_2 water-gas shift catalysts due to shutdown/startup modes for fuel cell applications. Appl Catal B: Environ 2005;56:69–75.
[3] Ma D, Lund CRF. Assessing high-temperature water-gas shift membrane reactors. Ind Eng Chem Res 2007;342(4):711–7.
[4] Panagiotopoulou P, Kondarides DI. Effects of promotion of TiO_2 with alkaline earth metals on the chemisorptive properties and water-gas shift activity of supported platinum catalysts. Appl Catal B: Environ 2011;101:738–46.
[5] Babita K, Sridhar S, Raghavan KV. Membrane reactors for fuel cell quality hydrogen through WGSR – review of their status, challenges and opportunities. Int J Hydrogen Energy 2011;36:6671–88.
[6] Bi Y, Xu H, Li W, Goldbach A. Water-gas shift reaction in a Pd membrane reactor over Pt/Ce0.6Zr0.4O2 catalyst. Int J Hydrogen Energy 2009;34:2965–71.
[7] Augustine AS, Ma YH, Kazantzis NK. High pressure palladium membrane reactor for the high temperature water gas shift reaction. Int J Hydrogen Energy 2011;36:5350–60.
[8] Criscuoli A, Basile A, Drioli E. An analysis of the performance of membrane reactors for the water-gas shift reaction using gas feed mixtures. Cat Today 2000;56:53–4.
[9] Uemiya S, Sato N, Ando H, Kikuchi E. The water gas shift reaction assisted by a paladium membrane reactor. Ind Eng Chem Res 1991;30:585–9.
[10] Markatos NC, Vogiatzis E, Koukou MK, Papayannakos N. Membrane reactor modelling—a comparative study to

evaluate the role of combined mass and heat dispersion in large-scale adiabatic membrane modules. Chem Eng Res Des 2005;83(10A):1171–8.
[11] Brunetti A, Caravella A, Barbieri G, Drioli E. Simulation study of water gas shift reaction in a membrane reactor. J Membr Sci 2007;306:329–40.
[12] Adrover ME, López E, Borio DO, Pedernera MN. Simulation of a membrane reactor for the WGS reaction: pressure and thermal effects. Chem Eng J 2009;154(1–3):196–202.
[13] Cornaglia CA, Múnera JF, Lombardo E. Kinetic study of a novel active and stable catalyst for the water gas shift reaction. Ind Eng Chem Res 2011;50:4381–9.
[14] Hill Jr CG. An introduction to chemical engineering kinetics & reactor design. New York: John Wiley & Sons; 1977.
[15] Pozrikidis C. Numerical computation in science and engineering. New York: Oxford University Press; 1998.
[16] Gear CW. Numerical initial-value problems in ordinary differential equations. New York: Prentice-Hall; 1971.
[17] Vidal H, Bernal S, Baker R, Finol D, Pérez Omil JA, Pintado JM, Rodríguez-Izquierdo, J.M.. Characterization of La_2O_3/SiO_2 mixed oxide catalyst supports. J Catal 1999;183:53–62.
[18] Basile A, Criscuoli A, Santella F, Drioli E. Membrane reactor for water gas shift reaction. Gas Sep Purif 1996;10(4):243–54.
[19] Tosti S, Violante V, Basile A, Chiappetta G, Castelli S, De Francesco M, et al. Catalytic membrane reactors for tritium recovery for tritiated water in the ITER fuel cycle. Fusion Eng Des 2000;49–50:953–8.
[20] Adrover ME, López E, Borio DO, Pedernera MN. Theoretical study of a membrane reactor for the water gas shift reaction under non-isothermal conditions. AIChE J 2009;55:3206–13.
[21] Mendes D, Mendes A, Madeira LM, Iulianelli A, Sousa JM, Basile A. The water-gas shift reaction: from conventional catalytic systems to Pd-based membrane reactors – a review. Asia-Pac J Chem Eng 2010;5:111–37.
[22] Newsome DS, Kellog P. The water-gas shift reaction. Catal Rev Sci Eng 1980;21(2):275–318.

Nomenclature

a_v: external particle surface area per unit reactor volume, $m_p^2\ m_r^{-3}$
A_p: external particle surface area, m_p^2
A_T: cross sectional area of tubes, m^2
d_s: shell tube diameter, m
d_{te}: external tube diameter, m
d_p: particle diameter, m
F_{To}: total feed flow rate, mol s^{-1}
J_{H_2}: permeation flow of hydrogen, mol $s^{-1}\ m^{-2}$
k: surface reaction rate constant, $mol_{CO}\ kg_{cat}^{-1}\ s^{-1}$
K: equilibrium constant
$k_{g,i}$: mass transfer coefficient for component i, kmol $m_i^{-2}\ s^{-1}$ atm^{-1}
K_i: adsorption equilibrium constant for component i, k Pa^{-1}
L: tube length, m
L_m: membrane length, m
N: number of components (reaction side)
p_i: partial pressure of component i, atm
r_{CO}: reaction rate, $mol_{CO}\ kg_{cat}^{-1}\ s^{-1}$
S: selectivity
S_g: BET surface area, $m_p^2\ g^{-1}$
T: temperature, K
V_r: reactor volume, m_r^3
W: catalyst mass, g
y: molar fraction
z: axial coordinate, m

Greek letters

ε: porosity, $m_f^3\ m_r^{-3}$
ρ_B: bed density, $kg_{cat}\ m_r^{-3}$

Subscripts

CO: carbon monoxide
H_2: hydrogen
i: component i
o: at the axial coordinate z = 0
L: at the axial coordinate z = L
P: permeate
G: sweep gas

Superscripts

S: surface

Acronyms

WGS: water gas shift
MR: membrane reactor